Journal of Colloid and Interface Science 446 (2015) 218–225

Contents lists available at ScienceDirect

Journal of Colloid and Interface Science

www.elsevier.com/locate/jcis

Spreading of blood drops over dry porous substrate: Complete wetting case

Tzu Chieh Chao, Omid Arjmandi-Tash, Diganta B. Das, Victor M. Starov *

Department of Chemical Engineering, Loughborough University, Loughborough LE11 3TU, UK

GRAPHICAL ABSTRACT

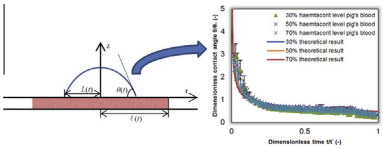

ARTICLE INFO

Article history:
Received 4 December 2014
Accepted 20 January 2015
Available online 28 January 2015

Keywords:
Dry blood spot sampling
Blood
Dry porous layer
Capillary spreading
Imbibition

ABSTRACT

Hypothesis: The process of dried blood spot sampling involves simultaneous spreading and penetration of blood into a porous filter paper with subsequent evaporation and drying. Spreading of small drops of blood, which is a non-Newtonian liquid, over a dry porous layer is investigated from both theoretical and experimental points of view.

Experiments and theory: A system of two differential equations is derived, which describes the time evolution of radii of both the drop base and the wetted region inside the porous medium. The system of equations does not include any fitting parameters. The predicted time evolutions of both radii are compared with experimental data published earlier.

Findings: For a given power law dependency of viscosity of blood with different hematocrit level, radii of both drop base and wetted region, and contact angle fell on three universal curves if appropriate scales are used with a plot of the dimensionless radii of the drop base and the wetted region inside the porous layer and dynamic contact angle on dimensionless time. The predicted theoretical relationships are three universal curves accounting satisfactorily for the experimental data.

1. Introduction

Dried blood spot (DBS) sampling is a method of blood collection, transportation and storage which has been investigated and used over the recent decades [1–6]. However, most studies of DBS have been focused on the clinical aspects, such as, developing new analytical method and improving their sensitivity of measurements, and the detection of new analytes. The mechanisms of blood spreading behavior during DBS sampling on DBS filter paper has not been investigated yet. The basic procedure of DBS sampling is to deposit a small but known amount of blood droplet on a filter paper where the droplet will spread, penetrate into and slowly dry out as a spotted sample. Hence, the sampling process can be described in terms of spreading of blood, which is a non-Newtonian fluid, over a thin porous substrate. In order to investigate the influence of the spreading/imbibition behavior on the DBS analysis, the development of a theoretical model is presented below.

The spreading of Newtonian liquids over smooth homogeneous surfaces has been investigated in [7–10]. It has been established that a singularity at the three phase contact line is removed by the action of surface forces [8,10]. The presence of roughness and/or a porous sublayer changes substantially the wettability of the substrate [11] and, hence, the spreading behavior [12–14]. The theoretical description of spreading over real surfaces is

* Corresponding author. Fax: +44 (0)1509 223923.
E-mail addresses: T.Chao@lboro.ac.uk (T.C. Chao), O.Arjmandi-Tash@lboro.ac.uk (O. Arjmandi-Tash), d.b.das@lboro.ac.uk (D.B. Das), v.m.starov@lboro.ac.uk (V.M. Starov).

http://dx.doi.org/10.1016/j.jcis.2015.01.054
0021-9797/

Nomenclature

Latin

a	radius of pores (μm)
A	dimensionless parameter (–)
b, c, C	integration constant (–)
g	gravity acceleration value (m s^{-2})
h	height of the drop (mm)
K_n	permeability of the porous layer (mD)
k	flow consistency index (Pa s^n)
L	radius of the drop base (mm)
ℓ	radius of the circular edge of the wetted region inside the porous layer (mm)
m	porosity (–)
p	pressure (Pa)
r, z	co-ordinate system (mm)
t, T	time (s)
u, v	vertical and radial velocity components (m/s)
V	volume of the drop (μl)

Greek

γ	interfacial tension (dyn cm^{-1})
σ	surface tension (dyn cm^{-1})
$\dot{\gamma}$	shear rate (s^{-1})
Δ	thickness of the porous layer (μm)
δ	small parameter (–)
η	effective viscosity (mPa s)
θ	dynamic contact angle (°)
ν	dimensionless parameter (–)
ρ	density (kg m^{-3})
λ	effective lubrication parameter (–)
χ	dimensionless parameter (Eqs. (28) and (29)) (–)

Subscripts

0	initial value
p	porous layer
g	ambient air
c	capillary
η	viscous
Δ	complete saturation of the porous layer in the vertical direction
f	marks the constant value of the contact angle over the duration of the second stage
+	expansion
−	shrinkage
d	drop
m	corresponds to the moment when the drop base reaches its maximum value

Superscripts

*	characteristic value
−	dimensionless

usually based on an *ad hoc* empirical "slippage condition" [15–19]. In [20] the spreading of small drops of Newtonian liquids over thin porous layers saturated with the same liquid has been investigated. Instead of the "slippage conditions" Brinkman's equations have been used in [20] for the description of the liquid flow inside the porous substrate. In [21] the spreading of Newtonian liquid over dry porous substrates was investigated in the case of complete wetting.

Spreading of droplets of non-Newtonian liquids over smooth solid surfaces was considered in [22] in the case of complete wetting. Considerable deviations from the spreading of Newtonian liquids were found [22]. In [23] a simultaneous spreading and evaporation of droplets of Newtonian liquids were considered.

Below the liquid under investigation is spreading/imbibition of a blood drop, which is a non-Newtonian power-law liquid, over a filter paper. Hence, the problem under investigation is similar to that considered in [21] when a drop of Newtonian liquid spreads over a dry porous layer, however, the difference is that now the liquid is a non-Newtonian blood. The experimental result on blood drops spreading over Whatman 903 filter paper (GE healthcare, UK) has been presented in [24]. The experimental results presented in [24] show that the blood spreading deviates from the corresponding Newtonian liquid [21] in two ways: (i) the droplets spreading governs by a different law as compared with [21] and (ii) non-Newtonian liquid imbibition into a porous substrate differs from that of Newtonian liquids.

The problem is treated below under the lubrication theory approximation and in the case of complete wetting. Spreading of "big drops", that is, bigger as compared with thickness of the porous substrate but still small enough to neglect the gravity action over "thin porous layers" is considered below.

2. Theory

The kinetics of blood motion in the drop both above and within the porous layer itself is taken into account below. It is assumed that the thickness of the porous layer, Δ, is much smaller than the drop height, that is, $\Delta \ll h^*$, where h^* is the scale of the drop height. The drop profile is assumed to have a low slope, $h^*/L^* \ll 1$, where L^* is the scale of the drop base, and the influence of the gravity is neglected (small drops, Bond number $\rho g L^{*2}/\gamma \ll 1$, where ρ, g, and γ are the liquid density, gravity acceleration and the liquid–air interfacial tension, respectively). That is, only capillary forces are taken into account.

Under such assumptions a system of two differential equations is deduced below, which describes the time evolution of the radii of both the drop base, $L(t)$, and the wetted region inside the porous layer, $\ell(t)$, (Fig. 1).

2.1. Droplet profile

According to [22] in the case of the capillary spreading the droplet profile in the central part of the droplet, except for a small vicinity of the three phase contact line, can be presented as a spherical cap even in the case of non-Newtonian liquids, which is similar to the case of Newtonian liquid [21]:

$$h(t,r) = \frac{2V}{\pi L^4}(L^2 - r^2), \quad r < L(t) \tag{1}$$

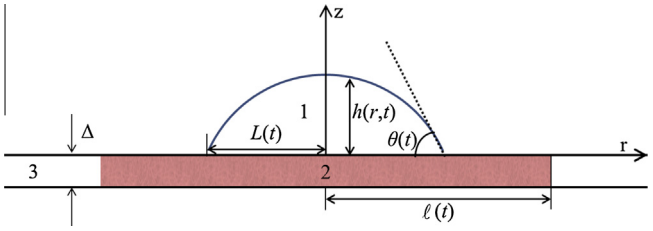

Fig. 1. Cross-section of the axis-symmetric spreading drop over initially dry filter paper with thickness Δ. 1 – liquid drop; 2 – wetted region inside the porous substrate; 3 – dry region inside the porous substrate. $L(t)$ – radius of the drop base; $\ell(t)$ – radius of the wetted area inside the porous substrate; Δ – thickness of porous substrate; $\theta(t)$ – contact angle; r, z co-ordinate system.

The latter expression is independent of the power law for the bulk viscosity.

The porous layer is assumed to be thin enough and the time for saturation in the vertical direction can be neglected relative to other time scales of the process.

Darcy's law cannot be used for description of the flow of a non-Newtonian liquid in the thin porous layer; hence, a modified approach is used (see the Supplementary Material for further details).

In the same way as in [21] the time required for a complete saturation of the porous layer in the vertical direction, t_{Δ}, can be estimated. Accordingly, the porous layer beneath the spreading drop ($0 < r < L(t)$) is always assumed completely saturated.

The capillary pressure inside the porous layer, p_c, can be estimated as $p_c \approx \frac{2\gamma}{a^*}$, where a^* is the scale of capillary radii inside the porous layer and γ is the surface tension. The capillary pressure inside the drop, $p - p_g$, can be estimated as $p - p_g \approx \frac{\gamma h^*}{L^{*2}} = \frac{h^*}{L^*}\frac{\gamma}{L^*} \ll \frac{\gamma}{L^*} \ll \frac{\gamma}{a^*} \approx p_c$, where p_g is the pressure in the ambient air. That is, the capillary pressure inside the drop can be neglected as compared with the capillary pressure inside the filter paper.

The drop volume, $V(t)$, changes over time, t, because of the imbibition of the liquid into the porous layer, this means:

$$V(t) = V_0 - \pi m \Delta \ell^2(t) \tag{2}$$

where V_0 is the initial volume of the drop; m is the porosity of the porous layer; and $\ell(t)$ is the radius of the wetted circle on the surface of the porous layer. The wetted region is a cylinder with radius $\ell(t)$ and the height Δ. $\ell(t)$ is referred below as the radius of the wetted region inside the porous layer.

Let t^* be the time instant when the drop is completely sucked by the porous substrate, $V(t^*) = 0 = V_0 - \pi m \Delta \ell^{*2}$, where ℓ^* is the maximum radius of the wetted region in the porous layer. The latter equation gives

$$\ell^* = \left(\frac{V_0}{\pi m \Delta}\right)^{1/2} \tag{3}$$

ℓ^* is used below to scale the radius of the wetted region in the porous layer, $\ell(t)$.

Eq. (1) gives the following value of the dynamic contact angle, θ, ($\tan\theta \approx \theta$):

$$\theta = \frac{4V}{\pi L^3} \tag{4}$$

or

$$L = \left(\frac{4V}{\pi\theta}\right)^{1/3} \tag{5}$$

2.2. Spreading above porous substrate

The drop motion is a superposition of two motions: (a) the spreading of the drop over already saturated part of the porous layer, which results in an expansion of the drop base, and (b) a shrinkage of the drop base caused by the imbibition into the porous layer. Hence, the following equation can be written:

$$\frac{dL}{dt} = v_+ - v_- \tag{6}$$

where v_+, v_- are unknown velocities of the expansion and the shrinkage of the drop base, respectively.

Let us take time derivative of both sides of Eq. (5). It results in:

$$\frac{dL}{dt} = -\frac{1}{3}\left(\frac{4V}{\pi\theta^4}\right)^{1/3}\frac{d\theta}{dt} + \frac{1}{3}\left(\frac{4}{\pi V^2\theta}\right)^{1/3}\frac{dV}{dt} \tag{7}$$

Over the whole duration of the spreading over the porous layer both the contact angle and the drop volume can only decrease with time. Accordingly, the first term in the right hand side of Eq. (7) is positive and the second one is negative.

Comparison of Eqs. (6) and (7) yields

$$v_+ = -\frac{1}{3}\left(\frac{4V}{\pi\theta^4}\right)^{1/3}\frac{d\theta}{dt} > 0, \quad v_- = -\frac{1}{3}\left(\frac{4}{\pi V^2\theta}\right)^{1/3}\frac{dV}{dt} > 0 \tag{8}$$

The derivation above can be justified as follows. There are two substantially different characteristic time scales in the problem under consideration: $T_\eta = t_\eta^* \ll t_p^* = T_p$, where t_η^* and t_p^* are time scales of the viscous spreading and the imbibition into the porous layer, respectively; $\delta = \frac{t_\eta^*}{t_p^*} \ll 1$ is a smallness parameter (around 0.08 for Newtonian fluid [21]). It is possible to write down $L = L(T_\eta, T_p)$, where T_η is a time of the fast viscous spreading and T_p is a time of the slower imbibition into the porous substrate. The time derivative of $L(T_\eta, T_p)$ is

$$\frac{dL}{dt} = \frac{\partial L}{\partial T_\eta} + \frac{\partial L}{\partial T_p} \tag{9}$$

Comparison of Eqs. (6), (8) and (9) shows that

$$v_+ = \frac{\partial L}{\partial T_\eta} = -\frac{1}{3}\left(\frac{4V}{\pi\theta^4}\right)^{1/3}\frac{d\theta}{dt}, \quad v_- = \frac{\partial L}{\partial T_p} = -\frac{1}{3}\left(\frac{4}{\pi V^2\theta}\right)^{1/3}\frac{dV}{dt} \tag{10}$$

The decrease of the drop volume, V, with time is determined solely by the imbibition into the porous substrate and, hence, the drop volume, V, only depends on the slow time scale.

According to the previous consideration the whole spreading process can be subdivided into two stages:

(i) first fast stage, when the imbibition into the porous substrate is small, and the drop spreads with approximately constant volume. This stage goes in the same way as the spreading over saturated porous layer and the arguments developed in [20] can be used here;
(ii) second slower stage, when the spreading process is almost over and the evolution is determined mostly by the imbibition into the porous substrate.

During the first stage the dependency of the droplet base radius can be rewritten in the following form [22]:

$$L(t) = \left[\frac{n}{2n+1}\frac{\lambda}{\alpha}\left(\frac{\sigma}{k}\right)^{1/n}\frac{V_0^{(n+2)/n}}{(2\pi)^{(n+2)/n}}(t+t_0)\right]^{\alpha} \tag{11}$$

where n is the flow behavior index from the known Otswald-de Waele relationship; $\alpha = \frac{n}{3n+7}$ and t_0 is the duration of the initial stage of spreading, when the capillary regime of spreading is not applicable; λ is a constant, which has been already determined from experimental data [20] for Newtonian liquids. Below the same value as in [20] was adopted for λ in the case of non-Newtonian liquids, because the actual viscosity of blood investigated was not drastically different from those liquids used in [20]. Note, the parameter λ is independent of the droplet volume [20]. The parameter α increases from 0 at $n = 0$ to 1/3 at $n \to \infty$ and equals to 0.1 in the case of Newtonian liquid at $n = 1$; that is, the limits are: $0 < \alpha < 1/3$.

In the case of Newtonian liquids Eq. (11) gives a well-known results of spreading in the case of complete wetting [8]: $L(t) \sim (t+t_0)^{0.1}$. Eq. (11) shows that pseudo plastic fluids, $n < 1$, spread slower than Newtonian liquids because in this case $0 < \alpha < 0.1$; however, dilatant fluids, $n > 1$, spread faster than Newtonian liquid because in this case $\alpha > 0.1$.

According to Eq. (11) the characteristic time scale of the first stage of spreading is

$$t_\eta^* = \frac{(2\pi)^{(n+2)/n} L_0^{1/\alpha}}{\frac{n}{2n+1}\frac{\lambda}{\alpha}\left(\frac{\sigma}{k}\right)^{1/n} V_0^{(n+2)/n}} \tag{12}$$

where $L_0 = L(0)$ is the radius of the droplet base in the end of the very fast initial stage of spreading. Eq. (11) can be rewritten now as

$$L(t) = L_0\left[\frac{t+t_0}{t_\eta^*}\right]^\alpha \tag{13}$$

Combination of Eqs. (13), (8) and (4) gives:

$$v_+ = \left(\frac{V(t)}{V_0}\right)^{1/3} \frac{\alpha L_0}{\left(\frac{t+t_0}{t_\eta^*}\right)^{1-\alpha} t_\eta^*} \tag{14}$$

Substitution of Eq. (2) into Eq. (8) gives the following expression for velocity of the drop base shrinkage, v_-:

$$v_- = \frac{2\pi^{2/3} m\Delta\ell}{3}\left(\frac{4}{(V_0 - \pi m\Delta\ell^2)^2\theta}\right)^{1/3}\frac{d\ell}{dt} \tag{15}$$

Substitution of the latter two equations into Eq. (6) results in:

$$\frac{dL}{dt} = \frac{\alpha\left(\frac{V}{V_0}\right)^{1/3}\left(\frac{n}{2n+1}\frac{\lambda}{\alpha}\left(\frac{\sigma}{k}\right)^{1/n}\frac{V_0^{(n+2)/n}}{(2\pi)^{(n+2)/n}}\right)^\alpha}{(t+t_0)^{1-\alpha}} - \frac{2\pi^{2/3} m\Delta\ell}{3}\left(\frac{4}{(V_0 - \pi m\Delta\ell^2)^2\theta}\right)^{1/3}\frac{d\ell}{dt} \tag{16}$$

The only unknown function left now is the radius of the wetted region inside the porous layer, $\ell(t)$, which is determined below.

2.3. Inside the porous layer outside the drop ($-\Delta < z < 0$, $L < r < \ell$)

The liquid flow inside the porous layer obeys the modified Darcy's law (Eq. (A.11) in Appendix A):

$$\frac{1}{r}\frac{\partial}{\partial r}\left(r\frac{\partial v}{\partial r}\right) = 0, \quad v = K_n\left(\frac{1}{k}\left|\frac{\partial p}{\partial r}\right|\right)^{1/n} \tag{17}$$

Solution of the latter equations is

$$p = -\left(\frac{c}{K_n}\right)^n k\frac{r^{1-n}}{1-n} + b, \quad v = \frac{c}{r} \tag{18}$$

where b and c are integration constants, which should be determined using the boundary conditions for the pressure at the drop edge, $r = L(t)$, and at the circular edge of the wetted region inside the porous layer, $r = \ell(t)$.

Note that in the case of the imbibition of a Newtonian liquid [21] the solution is different from the case of power law non-Newtonian liquids:

$$p = -(c\mu/K_p)\ln r + b; \quad v = \frac{c}{r} \tag{19}$$

because the solution, Eq. (18), becomes singular at n=1, that is, in the case of Newtonian liquid.

The boundary condition at the drop edge is:

$$p = p_g - p_c, \quad r = \ell(t) \tag{20}$$

where $p_c \approx \frac{2\gamma}{a^*}$ is the capillary pressure inside the pores of the porous layer, and a^* is a characteristic scale of the pore radii inside the porous layer.

The other boundary condition is

$$p = p_g + p_d, \quad r = L(t) \tag{21}$$

where p_d is an unknown pressure [21] inside the drop. It was estimated above and in [21] that $p_d \ll p_c$. That is, below p_d is omitted in expression (21).

Taking into account the latter two boundary conditions, both integration constants, b and c, can be determined, which gives the following expression for the radial velocity according to Eq. (18):

$$v = \frac{K_n}{r}\left[\frac{(1-n)(p_d + p_c)}{k(\ell^{1-n} - L^{1-n})}\right]^{1/n} \tag{22}$$

The velocity at the circular edge of the wetted region inside the porous layer is:

$$\frac{d\ell}{dt} = v|_{r=\ell} \tag{23}$$

Combination of the latter two equations gives the evolution equation for ℓ:

$$\frac{d\ell}{dt} = \frac{K_n}{\ell}\left[\frac{(1-n)p_c}{k(\ell^{1-n} - L^{1-n})}\right]^{1/n} \tag{24}$$

An estimation of the time scale t_p^* can be made according to Eq. (24) in the same way as in [21]:

$$t_p^* = \frac{\ell^{*(1+1/n)} k^{1/n}}{K_n p_c^{1/n}} \tag{25}$$

Comparison of the estimated values of t_η^* according to Eq. (12) and of t_p^* according to Eq. (25) shows that under all our experimental conditions the following inequality $t_\eta^* \ll t_p^*$ is really satisfied.

Substitution of Eq. (24) into Eq. (16) gives the following system of differential equations for the evolution of both the radius of the drop base, $L(t)$, and that of the wetted region inside the porous layer, $\ell(t)$:

$$\frac{dL}{dt} = \frac{\alpha\left(\frac{V}{V_0}\right)^{1/3}\left(\frac{n}{2n+1}\frac{\lambda}{\alpha}\left(\frac{\sigma}{k}\right)^{1/n}\frac{V_0^{(n+2)/n}}{(2\pi)^{(n+2)/n}}\right)^\alpha}{(t+t_0)^{1-\alpha}} - \frac{2L\pi m\Delta}{3}\frac{K_n}{V_0 - \pi m\Delta\ell^2}\left[\frac{(1-n)p_c}{k(\ell^{1-n} - L^{1-n})}\right]^{1/n} \tag{26}$$

$$\frac{d\ell}{dt} = \frac{K_n}{\ell}\left[\frac{(1-n)p_c}{k(\ell^{1-n} - L^{1-n})}\right]^{1/n} \tag{27}$$

Let us make the system of differential Eqs. (26), (27) dimensionless using new scales $\bar{L} = L/L_m, \bar{\ell} = \ell/\ell^*, \bar{t} = t/t^*$, where L_m is the maximum value of the drop base, which is reached at the unknown time instant t_m, that is, at the moment when the right hand site of Eq. (26) is equal to zero. Note that the time instant t^* is unknown but according to the previous estimations is not very much different from the characteristic time t_p^* according to Eq. (25). That is we adopt that $t^* = \nu t_p^*$, where ν is an unknown parameter, which can depend on n.

The same symbols are used for dimensionless variable (marked with an over-bar) as for corresponding dimensional variables. The system of Eqs. (26), (27) transforms as:

$$\frac{d\bar{L}}{d\bar{t}} = \frac{\nu A(1-\bar{\ell}^2)^{1/3}}{(\bar{t}+\bar{t}_0)^{1-\alpha}} - \frac{2\bar{L}}{3}\frac{\nu}{1-\bar{\ell}^2}\left[\frac{(1-n)}{(\bar{\ell}^{1-n} - \chi\bar{L}^{1-n})}\right]^{1/n} \tag{28}$$

$$\frac{d\bar{\ell}}{d\bar{t}} = \frac{\nu}{\bar{\ell}}\left[\frac{(1-n)}{(\bar{\ell}^{1-n} - \chi\bar{L}^{1-n})}\right]^{1/n} \tag{29}$$

where

$$\bar{t}_0 = t_0/t^* \ll 1, \quad \chi = \left(\frac{L_m}{\ell^*}\right)^{1-n},$$
$$A = \frac{2}{3}\frac{(\bar{t}_m + \bar{t}_0)^{1-\alpha}}{(1-\bar{\ell}_m^2)^{4/3}\left(\frac{\bar{\ell}_m^{1-n}-\chi}{1-n}\right)^{1/n}}, \quad \bar{\ell}_m = \frac{\ell_m}{\ell^*} \tag{30}$$

where ℓ_m is the radius of wetting region at the time instant t_m.

Eqs. (28) and (29) are a system of two first order differential equations, and, hence, two initial conditions should be imposed for solving them. These initial conditions should be initial conditions for both $\bar{L}(0)$ and $\bar{\ell}(0)$. The system of differential Eqs. (28) and (29) is singular at zero values of both $\bar{L}(0)$ and $\bar{\ell}(0)$. Hence a small but non-zero values were selected instead:

$$\bar{L}(0) = 0.001 \tag{31}$$

$$\bar{\ell}(0) = 0.001 \tag{32}$$

that is, very small values. The small initial time, $\bar{t}_0$, was selected as $\bar{t}_0 = 0.00001$. The calculation below shows that the result almost independent of the small initial values selected.

Solution of Eqs. (28) and (29) should satisfy the following four extra conditions:

$$\bar{L}(1) = 0 \tag{33}$$

$$\bar{L}(\bar{t}_m) = 1 \tag{34}$$

$$\frac{d\bar{L}(\bar{t}_m)}{d\bar{t}} = 0 \tag{35}$$

$$\bar{\ell}(1) = 1 \tag{36}$$

Conditions (34) and (35) were used above to select an expression for A and conditions (33) and (36) are to be satisfied. However, the system of differential Eqs. (28) and (29) includes two unknown dimensionless parameters, χ, v, and precisely two extra conditions (33) and (36) to determine these unknown parameters.

According to Eqs. (10) and (28) the dimensionless velocities of the expansion of the drop base, $\bar{v}_+$, and the shrinkage, $\bar{v}_-$, are:

$$\bar{v}_+ = \frac{vA(1-\bar{\ell}^2)^{1/3}}{(\bar{t}+\bar{t}_0)^{1-\alpha}}, \bar{v}_- = \frac{2\bar{L}}{3}\frac{v}{1-\bar{\ell}^2}\left[\frac{(1-n)}{(\bar{\ell}^{1-n}-\chi\bar{L}^{1-n})}\right]^{1/n} \tag{37}$$

Let us rewrite Eq. (4) using the same dimensionless variables and $\overline{V} = V/V_0 = 1-\bar{\ell}^2$:

$$\theta = \frac{4V_0}{\pi L^3}(1-\bar{\ell}^2) \tag{38}$$

Let us introduce $\theta_m = \frac{4V_0}{\pi L_m^3}(1-\bar{\ell}_m^2)$, which is the value of the dynamic contact angle at the time instant when the maximum value of the drop base is reached. Then Eq. (38) can be rewritten as:

$$\frac{\theta}{\theta_m} = \frac{(1-\bar{l}^2)/(1-\bar{l}_m^2)}{\bar{L}^3} \tag{39}$$

and the latter relationship should be a universal function of the dimensionless time, $\bar{t}$.

Let us consider the asymptotic behavior of system (26) and (27) during the second stage of the spreading. According to the previous consideration and as it will be confirmed below in Fig. 3, over the second stage of the spreading velocity of the expansion of the drop base, v_+, become small and, hence, to understand the asymptotic behavior the term corresponding to v_+ in the left hand side of Eq. (26) is omitted. This results in:

$$\frac{dL}{dt} = -\frac{2L\pi m\Delta}{3}\frac{K_n}{V_0-\pi m\Delta\ell^2}\left[\frac{(1-n)p_c}{k(\ell^{1-n}-L^{1-n})}\right]^{1/n} \tag{40}$$

while Eq. (27) is left unchanged. The system of differential Eqs. (27), (40) can be solved analytically. For this purpose Eq. (40) is divided by Eq. (27), which gives $\frac{dL}{d\ell} = -\frac{2\pi m\Delta L\ell}{3(V_0-\pi m\Delta\ell^2)}$. If $V = V_0 - \pi m\Delta\ell^2$ is used instead of ℓ, the latter equation takes the following form: $\frac{dL}{dV} = \frac{L}{3V}$, which can be easily integrated and the solution is

$$V = CL^3 \tag{41}$$

where C is an integration constant. Let us rewrite Eq. (4) using the same dimensionless variables and $\overline{V} = V/V_0$:

$$\overline{V} = \frac{\pi L_m^3}{4V_0}\theta\bar{L}^3 \tag{42}$$

Comparison of Eqs. (41) and (42) shows that the dynamic contact angle asymptotically remains constant during the second stage. This constant value is marked below as θ_f. It is necessary to emphasize that in the case under consideration the constancy of the contact angle during the second stage has nothing to do with the contact angle hysteresis: there is no hysteresis in our system here: θ_f is not a receding contact angle but forms as a result of a self-regulation of the flow in the drop-porous layer system [21].

3. Experimental data

3.1. Spreading behavior

All experimental data for our theoretical calculations were taken from the previous published paper [24], where a series of experiments on blood spreading were reported. Pig's blood was collected in EDTA anti-coagulated tubes (International Scientific Supplies Ltd. Bradford, UK) from a local butcher and prepared blood sample of different haematocrit levels [24]: 30%, 50%, 70%. Fig. 1 shows a cross-section of the axis-symmetric spreading drop over the porous medium with thickness Δ. The time evolution of the spreading radius, $L_{exp}(t)$, the droplet height, $h_{exp}(t)$, and the wetting region radius, $\ell_{exp}(t)$, were monitored [24]. According to [24] the pores structure of DBS sampling cards (filter paper) proves that the porous medium (DBS card) have a bi-porous structure, i.e., the macro size pores between the fibers and micro pores inside the fibers. The fast penetration in large pores, between the fibers, currently is only process taken into account according to the model above. However, there are two additional processes, which might influence the penetration of blood inside the porous medium: (i) the penetration inside the fibers, and (ii) adsorption of red blood cells on/inside fibers.

3.2. Blood rheology

Blood is a non-Newtonian liquid, which shows a shear-thinning behavior [24–26]. Different rheological models have been used based on curve fitting of experimental data for a description of the blood rheology [27–29]. The blood rheology measurements have been made in the previous publication [24] using the rheometer with plane geometry (4 cm diameter, stainless steel) and 250 μm gap. The viscosity measurements have been made in shear range 0.2–100 s^{-1} in [24]. The power law equation known as Otswald- de Waele relationship has been used as the rheological model of blood:

$$\eta = k\dot{\gamma}^{n-1} \tag{43}$$

where k is the termed "flow consistency index", n is the "flow behavior index" and $\dot{\gamma}$ is the shear rate. Eq. (43) showed a good agreement with previous experimental measurement of blood viscosity [24], where both k and n were determined for all haematocrit levels under investigation.

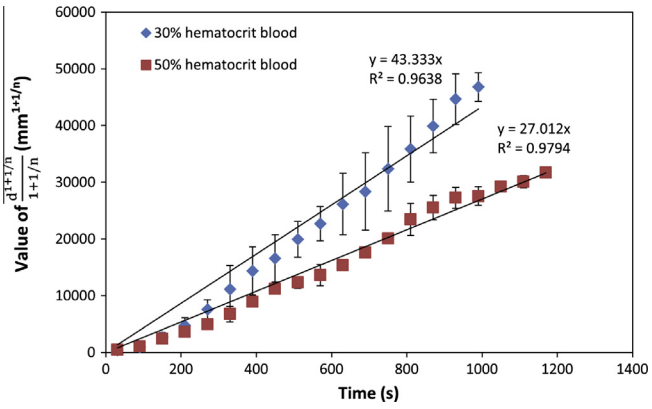

Fig. 2. The time evolution of $\frac{d^{1+1/n}(t)}{1+1/n}$ for different haematocrit level pig's blood.

3.3. Independent determination of $\frac{K_n p_c^{1/n}}{k^{1/n}}$

As mentioned above the permeability of porous layer and effective capillary pressure are considered as a single coefficient in our theoretical model. In order to determine this coefficient, additional experiments were carried out to obtain this coefficient based on the modified Darcy's law. The horizontal imbibition of blood samples with different haematocrit levels into the filter paper was used similar to [21]. The filter paper used in the spreading experiment were cut into rectangular sheets of 1.5 cm $*$ 3.0 cm. The depth of immersed part of each sheet was around 0.3–0.5 cm into the blood container and the position of imbibition front was recorded by high speed camera over time. According to Eq. (17) the position of the imbibition front can be expressed in the following way:

$$d^{1+1/n}(t) = \frac{K_n p_c^{1/n}}{k^{1/n}}(1+1/n)t \tag{44}$$

where $d(t)$ is the position of the imbibition front inside the filter paper. It was found that in all runs $d^{1+1/n}(t)$ proceeds along a straight line, whose slope gives $\frac{K_n p_c^{1/n}}{k^{1/n}}$ value as shown in Fig. 2.

The measured values of $\frac{K_n p_c^{1/n}}{k^{1/n}}$ are presented in Table 1.

4. Numerical solution of Eqs. (28) and (29)

The system of differential Eqs. (28) and (29) was solved using initial conditions (31) and (32). The two unknown parameters χ, v were determined using additional conditions (33) and (36). Note that the system after that does not include any fitting parameters. According to our calculations both parameters, χ, v, vary insignificantly for all three n values used (Table 2).

Hence, the three dimensionless dependencies $\bar{L}(\bar{t}), \bar{\ell}(\bar{t})$ and θ/θ_m should fall on three almost universal curves. See solid lines in Figs. 4–6. This conclusion is in a good agreement with our experimental observations (see below): experimental dependencies also show a universal behavior.

Table 1
The value of $\frac{K_n p_c^{1/n}}{k^{1/n}}$ for different haematocrit level of blood.

Haematocrit level (%)	$\frac{K_n p_c^{1/n}}{k^{1/n}}$ (mm$^{(1+1/n)}$ s^{-1})
30	43.333 ± 6.504
50	27.012 ± 1.407
70	N/A

Table 2
Calculated values of two unknown dimensionless parameters χ, v. The values of n were determined in [24].

Haematocrit level (%)	n	ν	χ
30	0.394	0.281	0.376047
50	0.368	0.2439	0.3747172
70	0.325	0.214	0.3454006

5. Results and discussion

The time evolution of radius of blood droplet at constant volume, 10 ± 0.5 μl, spreading on Whatman 903 filter paper and the time evolution of the radius of wetting region have been presented earlier in [24]. The droplet radius of all the blood samples reached zero at the end of spreading/imbibition process. Although there are some differences of spreading behavior between the blood samples with different haematocrit level spreading on DBS filter paper, in general, the spreading results of all samples showed similar features during the whole spreading process. The whole process can be subdivided into two stages as in the case of Newtonian liquids [21]: over duration of the first stage, the expansion of droplet radius, due to the capillary regime of spreading, is faster than the shrinkage, due to the imbibition into the filter paper, until they counterbalance themselves as the maximum radius is reached. After that the second stage begins where the droplet base starts to shrink and the wetted region expands until the droplet disappears.

In all spreading experiments [24] the drops shape remained a spherical cap over the entire duration of spreading which showed a good agreement with our theoretical assumption above. This spherical cap shape allowed calculating the dynamic contact angle of each spreading droplet [24]. The dynamic contact angle of all samples decreased rapidly during first stage of spreading as well as the radius of droplet base increased. After the spreading radius reached its maximum value, $L_{m,\mathrm{exp}}$, the dynamic contact angle levelled off and remained a constant value over duration of the second stage.

Table 3 provides the experimental data obtained from spreading experiment [24], which include the maximum spreading radius, $L_{m,\mathrm{exp}}$, the time of complete imbibition, t^*_{exp}, contact angle, $\theta_{m,\mathrm{exp}}$, and ℓ^*_{exp}.

Experimental dependences of radius of the drop spreading, L_{exp}, radius of the wetted area, ℓ_{exp}, contact angle, θ_{exp}, were made dimensionless using the values presented in Table 3.

Fig. 3 shows dimensionless velocity $\bar{v}_+$ and $\bar{v}_-$ of different haematocrit level blood spreading over Whatman 903 filter paper calculated according to Eq. (37). Fig. 3 confirms that:

(a) first stage is very shorter as compared with the second stage of spreading/imbibition. The capillary spreading prevails on

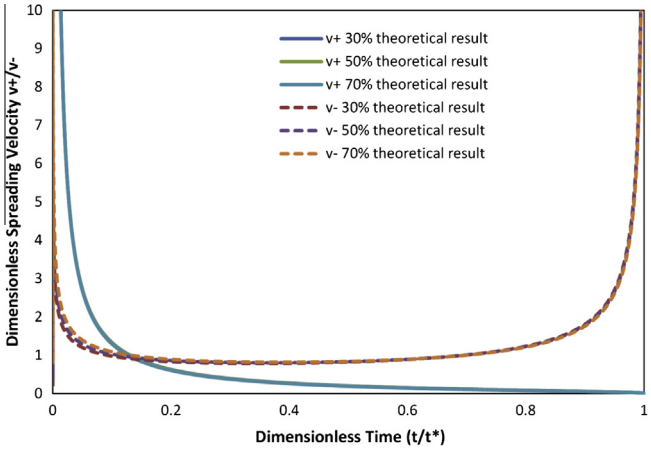

Fig. 3. The time evolution of the dimensionless velocity $\bar{v}_+$ and $\bar{v}_-$ according to Eq. (37) for blood samples with 30%, 50% and 70% haematocrit level.

Table 3
The experimental values used to make experimental dependences dimensionless for comparison with predicted time dependences according to Eqs. (28), (29) and (39) from [24].

	t^*_{exp} (s) Time of complete imbibition	$L_{m,exp}$ (mm) Maximum spreading radius of droplet base	$\theta_{m,exp}$ (°) Contact angle at maximum spreading	ℓ^*_{exp} (mm) Maximum radius of wetting region
30% haematocrit level	0.351 ± 0.014	2.18 ± 0.07	32.80 ± 1.88	3.36 ± 0.09
50% haematocrit level	0.508 ± 0.022	2.18 ± 0.08	30.94 ± 2.50	3.32 ± 0.06
70% haematocrit level	0.663 ± 0.027	2.09 ± 0.09	33.48 ± 2.37	3.20 ± 0.04

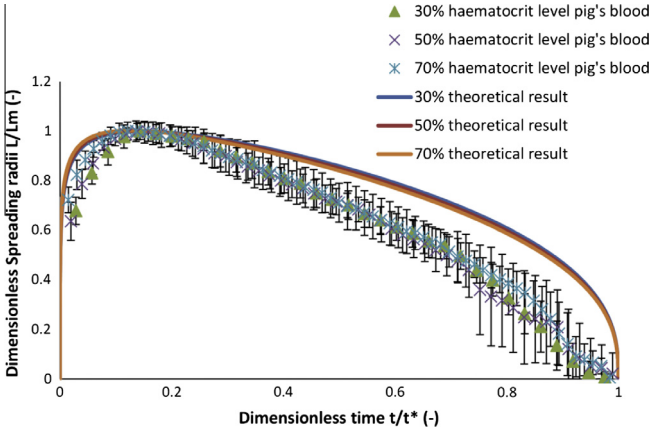

Fig. 4. The simulation result of the dimensionless time evolution of radius of blood droplet. Theoretical results according to Eqs. (28) and (29). Experimental data from [24].

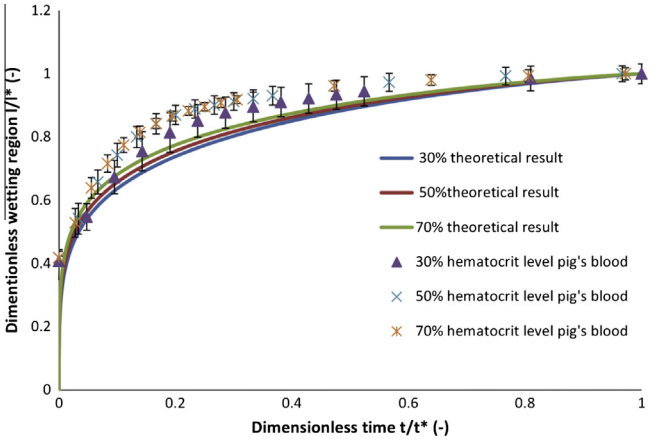

Fig. 5. Time evolution of radius of the wetted area inside porous substrate. Theoretical results according to Eqs. (28) and (29). Experimental data from [24].

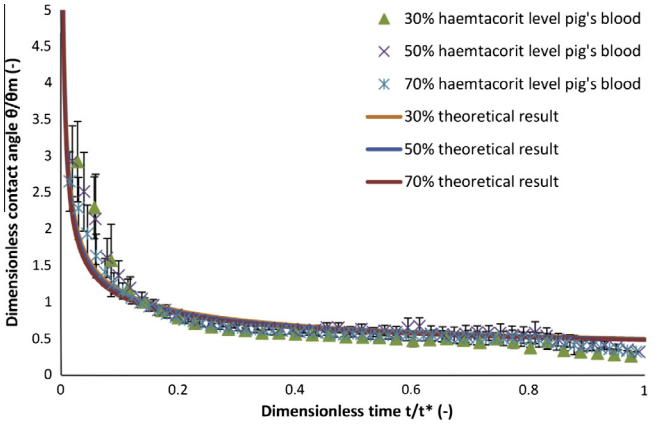

Fig. 6. The time evolution of contact angle of blood droplet with different haematocrit levels on porous substrate. The solid curve calculated according to Eq. (39). Experimental data from [24].

this stage over the drop base shrinkage caused by the liquid imbibition into the porous substrate;

(b) spreading of the drop almost stops after the first stage of spreading and the shrinkage of the drop base is determined by the suction of the liquid from the drop into the porous substrate.

The main results of comparison of experimental and calculated dependences according to Eqs. (28), (29), (39) are presented in Figs. 4–6. These figures show that all the data fall into corresponding universal curves when the dimensionless values are used: L/L_m, ℓ/ℓ^*, t/t^*, and θ/θ_m. The measured values of the corresponding experimental values $L_{m,exp}$, ℓ^*_{exp} and t^*_{exp} for all experimental runs are given in Table 2. It shows that the dimensionless time $\bar{t}_{m,exp}$ is about $0.14 \approx \delta$. Solid curves in Figs. 4–6 represent the solution of the system of differential Eqs. (28), (29) and Eq. (39) for different values of n. Figs. 4–6 shows that the developed theory results in a reasonable prediction of experimental dependences. However, the main conclusion is that both experimental dependences and the calculated theoretical dependences show a remarkable universal behavior independent of n.

It is necessary to take into account that we used a simple model of blood rheology and its penetration into the porous substrate: we did not take into account absorption of red blood cells (RBC) inside the porous substrate, bi-porous structure of the substrate, and evaporation.

Calculated dependences presented in Figs. 4–6 (solid curves) show that the shape of these dependences is independent of small values selected as initial conditions according to (31) and (32).

In order to predict completely the blood spot behavior, the four experimental data, time of complete imbibition t^*, maximum radius of droplet base, L_m, maximum radius of wetting region, ℓ^* and contact angle at maximum spreading, θ_m, have to be determined from our simulated result and physical parameters which are obtained independently from different experiments. These physical parameters are the viscosity of blood, $\eta = k\dot{\gamma}^{n-1}$, namely, n and k; the interfacial tension, σ and the physical parameters of porous substrate: the permeability coefficient, $K_n p_c^{1/n}$, the thickness, Δ, and the porosity, m. The universal dimensionless constants, namely, $\nu, \chi, \bar{t}_m, \bar{\ell}_m$, could be determined from the result of our dimensionless model.

The value ℓ^* can be determined directly according to Eq. (3), where the values of V_0, m and Δ are equal to 10 ± 0.5 μl, 0.57 ± 0.03 and 500 ± 50 μm, respectively [24]. The imbibition time, t^*, can be obtained by $t^* = \nu t^*_p$, where t^*_p is determined by Eq. (25) and the measured values of $\frac{K_n p_c^{1/n}}{k^{1/n}}$ in Table 1.

Due to the fast expansion of blood drop spreading, the imbibition of blood could be neglected during the first stage of spreading; hence, the maximum spreading radius can be approximately approached by Eq. (11) and accordingly, the contact angle, θ_m can be indicated by Eq. (38) as the following equations:

$$L_m = \left[\frac{n}{2n+1}\frac{\lambda}{\alpha}\left(\frac{\sigma}{k}\right)^{1/n}\frac{V_0^{(n+2)/n}}{(2\pi)^{(n+2)/n}}t^*(\bar{t}_m + \bar{t}_0)\right]^{\alpha} \quad (45)$$

Table 4
The predicted values of blood spot spreading behavior calculated from simulated result and physical properties of blood and porous substrate.

	t^*_{sim} (s) Time of complete imbibition	$L_{m,sim}$ (mm) Maximum spreading radius of droplet base	$\theta_{m,sim}$ (°) Contact angle at maximum spreading	ℓ^*_{sim} (mm) Maximum radius of wetting region
30% haematocrit level	0.464 ± 0.220	2.050 ± 0.096	44.30 ± 8.37	3.344 ± 0.255
50% haematocrit level	0.803 ± 0.297	1.957 ± 0.082	49.61 ± 8.65	3.344 ± 0.255
70% haematocrit level	N/A	N/A	N/A	3.344 ± 0.255

$$\theta_m = \frac{4V_0}{\pi L_m^3}(1-\bar{\ell}_m^2) \tag{46}$$

where $\sigma \cong 50 \pm 5$ dyne/cm and the values of the k and n for different haematocrit levels are presented in [24].

All the calculated data for the maximum spreading radius, $L_{m,sim}$, the time of complete imbibition, t^*_{sim}, contact angle, $\theta_{m,sim}$, and ℓ^*_{sim} based on the simulation result and independent measurements of physical parameters are shown in Table 4. The comparison of simulated and experiment result demonstrates that the simulated prediction is in a good agreement with our experimental observation.

6. Conclusions

The process of dried blood spot sampling involves simultaneous spreading and penetration of blood into a porous filter paper with subsequent evaporation and drying. Spreading of small drops of blood, which is a non-Newtonian liquid, over a dry porous layer is investigated from both theoretical and experimental points of view. A system of two differential equations is derived from the combination of the model of spherical cap spreading over porous layer [21] and a modified Darcy's law for power law fluids. It describes the time evolution of radii of both the drop base and the wetted region inside the porous layer in the course of blood spreading over a dry porous substrate. The deduced system of differential equation does not include any fitting parameters and predict a universal behavior of the dimensionless dependences of the radii of the droplet base and wetted area inside the porous substrate, and contact angle, which are almost completely independent of the rheological properties of blood. The time evolution of the radii of the drop base and the wetted region inside the porous layer, and dynamic contact angle were monitored in [24] for power law dependency of the viscosity of blood. All experimental data fell on three universal curves if appropriate scales are used with a plot of the dimensionless radii of the drop base and the wetted region inside the porous layer, and the dynamic contact angle of the drop on dimensionless time. The predicted theoretical relationships are three universal curves accounting quite satisfactory for the experimental data. The simulated results show a good agreement with experiment data although the bi-porous structure of the filter paper and adsorption of red blood cells inside the porous substrate were not taken into account according to the suggested model.

Acknowledgments

O. Arjmandy-Tash's and V. Starov's research was supported by Engineering and Physical Sciences Research Council, UK, CoWet Marie Curie ITN Project, EU and COST MP1106 project. Tzu Chieh Chao's research was supported by Department of Chemical Engineering Loughborough University, UK.

Appendix A. Supplementary material

Supplementary data associated with this article can be found, in the online version, at http://dx.doi.org/10.1016/j.jcis.2015.01.054 or by contacting the corresponding author.

References

[1] R. Meesters, G. Hooff, Bioanalysis (2013) 2187–2208.
[2] P.M. Edelbroek, J. Van der Heijden, L.M.L. Stolk, Therap. Drug Monitor. 31 (3) (2009) 327–336.
[3] P.A. Demirev, Anal. Chem. 85 (2) (2013) 779–789.
[4] I.J.M. Snijdewind, J.J.a. van Kampen, P.L.a. Fraaij, M.E. van der Ende, A.D.M.E. Osterhaus, R.A. Gruters, Antiviral Res. 93 (3) (2012) 309–321.
[5] S. Tanna, G. Lawson, Anal. Meth. 3 (8) (2011) 1709.
[6] S. Lehmann, C. Delaby, J. Vialaret, J. Ducos, C. Hirtz, Clin. Chem. Lab. Med.: CCLM/FESCC 51 (10) (2013) 1897–1909.
[7] P. De Gennes, Rev. Modern Phys. (1985)
[8] V. Starov, V. Kalinin, J. Chen, Adv. Colloid Interface Sci. 50 (1994) 187–221.
[9] T. Blake, J. Haynes, J. Colloid Interface Sci. 80 (3) (1969) 421–423.
[10] G.F. Teletzke, H. Ted Davis, L.E. Scriven, Chem. Eng. Commun. 55 (1–6) (1987) 41–82.
[11] M. Taniguchi, J. Pieracci, G. Belfort, Langmuir 10 (2001) 4312–4315.
[12] A. Aradian, E. Raphael, P. De Gennes, Eur. Phys. J. E 376 (2000) 367–376.
[13] a. Zadražil, F. Stepanek, O.K. Matar, Imbibition Solid. Porous Media 562 (2006) 1.
[14] F. Bacri, L. Brochard-Wyart, Eur. Phys. J. E 3 (2000) 87–97.
[15] P. Neogi, C. Miller, J. Colloid Interface Sci. 92 (2) (1983) 338–349.
[16] G. Beavers, D. Joseph, J. Fluid Mech. (1967)
[17] H. Greenspan, J. Fluid Mech. 84 (1978).
[18] S.H. Davis, L.M. Hocking, Phys. Fluids 11 (1) (1999) 48.
[19] S.H. Davis, L.M. Hocking, Phys. Fluids 12 (7) (2000) 1646.
[20] V.M. Starov, S.R. Kosvintsev, V.D. Sobolev, M.G. Velarde, S.a. Zhdanov, J. Colloid Interface Sci. 246 (2) (2002) 372–379.
[21] V.M. Starov, S.R. Kostvintsev, V.D. Sobolev, M.G. Velarde, S.a. Zhdanov, J. Colloid Interface Sci. 252 (2) (2002) 397–408.
[22] V.M. Starov, a.N. Tyatyushkin, M.G. Velarde, S.a. Zhdanov, J. Colloid Interface Sci. 257 (2) (2003) 284–290.
[23] S. Semenov, A. Trybala, R.G. Rubio, N. Kovalchuk, V. Starov, M.G. Velarde, Adv. Colloid Interface Sci. (2013)
[24] T.C. Chao, A. Trybala, V. Starov, D.B. Das, Colloids Surf. A: Physicochem. Eng. Aspects 451 (2014) 38–47.
[25] O.K. Baskurt, H.J. Meiselman, Seminars Thrombosis Hemostasis 29 (5) (2003) 435–450.
[26] E. Merrill, Physiol. Rev. 49 (4) (1969).
[27] F. Yilmaz, A critical review on blood flow in large arteries; relevance to blood rheology, viscosity models, and physiologic conditions 20(4) (2008) 197–211.
[28] A. Marcinkowska-Gapińska, J. Gapinski, W. Elikowski, F. Jaroszyk, L. Kubisz, Med. Biol. Eng. Comput. 45 (9) (2007) 837–844.
[29] A. Sequeira, J. Janela, An overview of some mathematical models of blood rheology, A Portrait of State-of-the-Art Research at the ..., 2007, pp. 65–87.